International Journal of Multiphase Flow 37 (2011) 12–23

Contents lists available at ScienceDirect

International Journal of Multiphase Flow

journal homepage: www.elsevier.com/locate/ijmulflow

Characterization and prediction of two-phase flow regimes in miniature tubes

Emil Rahim [a], Remi Revellin [b], John Thome [c], Avram Bar-Cohen [a,*]

[a] Thermal Packaging of Electronic and Photonic Systems (TherPES), Department of Mechanical Engineering, University of Maryland, College Park, MD 20742, USA
[b] Université de Lyon, CNRS; INSA-Lyon, CETHIL, UMR5008, F-69621 Villeurbanne, France; Université Lyon 1, F-69622, France
[c] Laboratory of Heat and Mass Transfer, Ecole Polytechnique Fédérale de Lausanne, LTCM-IGM-STI, EPFL, Mail 9, CH-1015 Lausanne, Switzerland

ARTICLE INFO

Article history:
Received 3 October 2009
Received in revised form 31 August 2010
Accepted 2 September 2010
Available online 17 September 2010

Keywords:
Miniature tubes
Flow patterns

ABSTRACT

Visual observations of two-phase regimes for R134a and R245fa flowing in 0.509 mm and 0.790 mm horizontal tubes are documented and compared to the predictions of the analytical flow regime models available in the literature. Annular flow was found to dominate the behavior of these two miniature channels, with a significant Slug flow regime at intermediate qualities. Despite the horizontal orientation of these tubes, there were no observations of Stratified flow and a very limited region of Bubble flow. A comparison of the more than 2200 flow regime observations to the predictions of the Taitel–Dukler flow regime methodology revealed that 67% of the empirically observed flow pattern data were correctly identified. The Ullmann–Brauner model, based on an air–water database, correctly predicted the appropriate flow regime for 81% of the reported data. Proposed modifications in the Bubble-to-Slug and Slug-to-Annular transition criteria, respectively, were shown to provide a modest further improvement in the overall predictability to 90% of the observed data for the two refrigerants studied.

1. Introduction

Two-phase flow of refrigerants, undergoing phase change while flowing in miniature tubes and channels, is a viable, though as yet poorly predicted, technique for a wide range of thermal management applications. In the absence of proven, first-principles, predictive relations, empirically-derived correlations must be used to determine the heat transfer coefficients, pressure drops, and dryout limits prevailing in such miniature passages. However, the paucity and large variance in the currently available two-phase data for the microchannel flow of refrigerants and dielectric liquids severely compromise the accuracy of such predictions. As with the two-phase flow pattern based flow boiling model of Kattan et al. (1998) for macrochannels, considerable insight, and some greater confidence and accuracy in the application of available thermo-fluid correlations, can be obtained by determining the prevailing flow regimes and associated heat transfer behavior of these microchannels. The present study, examining the predictive accuracy of the Taitel–Dukler and related flow regime categorizations for refrigerant flow in two miniature channels, provides an important first step in this process.

The flow of vapor and liquid in a channel can take various forms depending on the distribution and extent of aggregation of the two phases, with each distinct vapor/liquid distribution referred to as a "flow regime". Four primary two-phase flow regimes: Bubble, Intermittent, Annular, and Stratified, as well as numerous sub-regimes, have been identified in the literature, e.g. Hewitt, 1982. Bubble flow is associated with a uniform distribution of small spherical bubbles within the liquid phase. Intermittent flow is characterized by the flow of liquid plugs separated by elongated gas bubbles – often in the shape of slugs or bullets – though sometimes more chaotically mixed. In Annular flow, a relatively thin liquid layer flows along the channel walls, while the vapor flows in the center of the channel, creating a vapor "core" which may also contain entrained droplets. In vertical channels with heat addition, where the vapor content increases in the flow direction, the Bubble regime is followed sequentially by the Intermittent and Annular regimes. In horizontal or near-horizontal, channels – in addition to the three regimes encountered in vertical channels – two-phase flow may also occur in a Stratified pattern in which the liquid flows along the lower surface and the vapor above. This Stratified flow pattern generally occurs at relatively low liquid and vapor flow rates and, as the flow rates increase, transitions into Intermittent or Annular flow.

A recent study by Harirchian and Garimella (2008) provided visualization of flow patterns in microchannels with a height of 400 μm and width ranging from 100 to 5850 μm, yielding a hydraulic diameter in the range from 160 to 750 μm. Bubble, Churn, and Annular flows were observed in all channels, with Annular flow dominating in the smallest channels and Bubble flow, reflecting the prevalence of nucleate boiling, most common in channels with larger diameters. Megahed and Hassan (2009) stud-

* Corresponding author.
E-mail address: abc@umd.edu (A. Bar-Cohen).

0301-9322/$ - see front matter © 2010 Elsevier Ltd. All rights reserved.
doi:10.1016/j.ijmultiphaseflow.2010.09.002

ied the two-phase flow of FC-72 in a multichannel microchannel, consisting of 45 channels with a height of 276 μm, and width of 225 μm. They observed Bubble flow at vapor qualities up to 0.12 and Slug–Intermittent flow following at qualities up to 0.2. Annular flow was found to dominate the behavior of channels operating at vapor qualities starting from 0.25. Cheng et al. (2008) have provided a comprehensive literature review on gas–liquid two-phase flow patterns and flow pattern maps at adiabatic and diabatic conditions. Based on a review of more than 200 papers, they concluded that greater effort was required to develop and validate objective and theoretically based flow-pattern transition criteria and flow maps for microscale channels.

As part of an ongoing study at the Laboratory for Heat and Mass Transfer at the EPFL, the two-phase flow characteristics of R134a and R245fa, flowing through 0.509 mm and 0.790 mm diameter glass channels, at pressures ranging from 665 kPa to 887 kPa for R134a and at 213 kPa for R245fa, were observed. In these experiments, the two-phase mixtures were generated in similarly-sized electrically-heated, stainless steel channels. The length of the micro-evaporator varied from 30 to 70 mm and the mass flux ranged from 200 to 2000 kg/m^{2}s, along with inlet subcooling of 2–7 K.

In the context of the Cheng et al. (2008) recommendation, the primary objective of the current study is to evaluate the extent to which the two-phase, miniature tube flow patterns observed in these experiments depart from, or agree with, the classical flow pattern predictions of Taitel (1990) unified flow regime model. The empirically-determined regime transitions are also compared to the recently proposed Ullmann and Brauner (2007) flow regime transitions, and to other possible modifications in the Bubble-to-Slug and Slug-to-Annular boundaries. These data have previously been compared to other wholly empirical flow pattern maps in Revellin et al. (2006) and Revellin and Thome (2007a). The data here are not compared to the recent theoretically based, coalescing bubble flow map of Revellin et al. (2008), since that map distinguishes only three flow regimes and not the traditional flow patterns identified in the present study.

2. Taitel–Dukler unified flow regime model

An appreciation for the dependence of thermo-fluid parameters on the form, as well as extent, of aggregation of each phase, led early researchers to describe and map the gas–liquid and vapor–liquid flow regimes prevailing in channels used to generate and/or transport two-phase flows. Earliest among these was the empirical flow regime map developed by Baker (1954) and numerous other attempts to develop a generalized flow regime map followed; notably Mandhane et al. (1974), Taitel and Dukler (1976), and Weisman et al. (1979).

Most noteworthy among these was the pioneering effort by Taitel and Dukler, defining and mapping the four predominant flow regimes (Stratified, Intermittent, Bubble, and Annular) with superficial gas and superficial liquid coordinates and proposing physics-based criteria for the transition from one regime to the next. After considerable additional contributions by Barnea et al. (1980), Shoham (1982), and Taitel and Dukler (1987), in 1990 this effort culminated in the Unified Model for predicting flow regime transitions in channels of any orientation, based on simple physical criteria and using familiar two-phase non-dimensional groupings. Fig. 1 displays such a map, using the Froude number (Eq. (1)), the T parameter (relating the liquid pressure drop to buoyancy, as in Eq. (2) below), and the Martinelli number (Eq. (3)) with the superimposed locus traced out by the data of Yang and Fujita (2004) for R113 flowing in micro gap channels, with the gap size ranging from 0.2 mm to 2 mm.

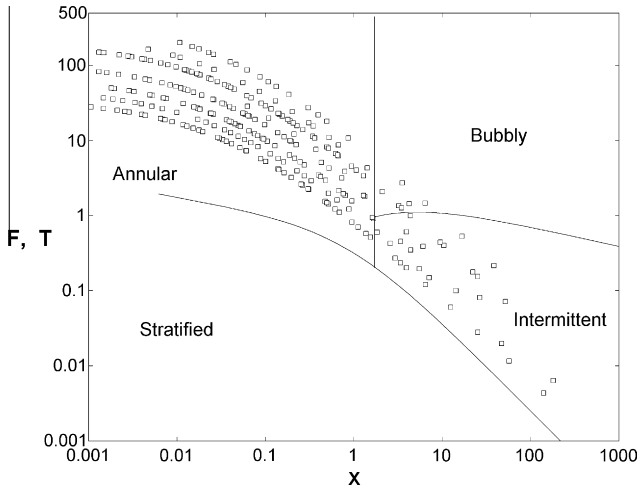

Fig. 1. Taitel–Dukler non-dimensional two-phase flow regime map for horizontal microgap channel (data of Yang and Fujita (2004): 0.2–2 mm gap, R113, G = 50–200 kg/m^{2}s, q = 20–90 kW/m^2).

$$F = \sqrt{\frac{\rho_G}{\rho_L - \rho_G}} \frac{U_{SG}}{Dg\cos\beta} \tag{1}$$

$$T = \left[\frac{[|dP/dx|_{SL}]}{(\rho_L - \rho_G)g\cos\beta}\right]^{1/2} \tag{2}$$

$$X = \left[\frac{[|dP/dx|_{SL}]}{[|dP/dx|_{SG}]}\right]^{1/2} \tag{3}$$

It is to be noted that the specific formulations used in developing the regime transition criteria reflect the distinction between surface tension driven regimes, such as Bubble and Intermittent flow, and shear force driven regimes, such as Stratified and Annular flow. The models contain little empiricism, and, therefore, can be applied to most fluids and be extrapolated to conditions other than water–air and water–steam flowing in the 25 mm and larger pipes that were used in the original experimental verification of the approach, Shoham (1982); Taitel and Dukler (1987).

In embracing the use of this flow regime map, it must, nevertheless, be recognized that the Taitel–Dukler methodology relies on adiabatic models that ignore the thermal interactions between phases, the pipe, and the environment all of which are present in diabatic systems, in which heat is added or extracted from the flowing two-phase mixture. Such an adiabatic model can be expected to provide better flow regime predictions as the applied heat flux decreases, Bar-Cohen et al. (1987). Nevertheless, the model has proven to be exceedingly useful for diabatic conditions and has demonstrated its first-order accuracy in numerous studies, including those performed by Taitel et al. (1978) and Frankum et al. (1997). Furthermore, it was the Taitel–Dukler map that was used by Kattan et al. (1998) to implement the heat flux effects on the flow-pattern transition boundaries for flow boiling in horizontal macroscale tubes.

Consequently, the physics-based models used in the Taitel and Dukler flow regime maps would appear to offer the best basis for determining the prevailing flow regimes in evaporating refrigerant and dielectric liquid flow within miniaturized channels and for facilitating the extrapolation of available macroscale correlations to such dielectric liquid microchannel coolers. It was found by Bar-Cohen and Rahim (2009) that the predictions of Taitel–Dukler methodology are in good agreement with the flow observations of an extensive data set generated from many published studies and that observed inflection points in the behavior of the two-phase

heat transfer coefficient often occur in proximity to the flow regime boundaries predicted by Taitel–Dukler.

Although the non-dimensional maps provide a compact way to represent specific transitions, for ease of interpretation and a more physical representation of the flow regime distribution, subsequent sections will use the dimensional form of the Taitel–Dukler flow regime map, with superficial velocity coordinates.

3. Ullmann–Brauner flow regime map

Recently, Ullmann and Brauner (2007) reexamined the effect of the channel diameter on the flow regime transitions and suggested that new mechanistic models be expressed in terms of the non-dimensional Eötvös number, Eo_D, defined as:

$$Eo_D = \frac{(\rho_L - \rho_V)gD^2}{8\sigma} \tag{4}$$

More specifically, Ullmann and Brauner suggested that in small Eötvös Number systems (of the order of 0.04), the negligibly small bubble velocity, even in vertical systems, leads to flow regimes resembling those obtained in conventional channels under microgravity conditions. They used the experimental flow regime data presented by Triplett et al. (1999) for air–water in 1.097 mm Pyrex pipe, corresponding to an Eötvös number of 0.021, to calibrate and determine the efficacy of this approach for small Eo_D configurations.

The Ullman–Brauner flow regime map describes five flow regimes; Dispersed Bubble, Bubble, Slug, Aerated Slug, and Annular, as will be shown later in this article.

3.1. Transition to dispersed bubble flow

The transition into the Dispersed Bubble regime was assumed to occur when the turbulence in the continuous phase is sufficient to stabilize the dispersed phase in the form of spherical bubbles. For liquid–vapor flow, the maximum bubble size, $d_{\max}$, should then be smaller than a critical size, d_{crit}, of coalescing bubbles. The maximum bubble size for a dilute dispersion of coalescing bubbles, $d_{\max,o}$, was estimated by Ullmann and Brauner by equating the momentum exerted by the turbulent eddy relative to the surface tension. Specifically, the maximum bubble size in a dense dispersion, $d_{\max,\varepsilon}$, was estimated based on equating the turbulent energy flux and the flux of the surface energy generated in the recurrently renewed dispersion. The greater value of these two estimates was taken as the maximum bubble size in the system.

The critical size of the coalescing bubble was taken as the smallest of three characteristic values: the size of a deformable bubble, $d_{c\sigma}$, the size of a floating bubble due to buoyancy, d_{cb}, and a value that was set as half the channel diameter. This transition was summarized by Ullmann and Brauner (2007) as follows:

$$d_{\max} = MAX\{d_{\max,o}, d_{\max,\varepsilon}\} \leqslant d_{crit} = MIN\{d_{c\sigma}, d_{cb}, 0.5D\} \tag{5}$$

3.2. Bubble-to-Slug flow transition

The Bubble-to-Slug transition value of the liquid superficial velocity was found as

$$U_L = \frac{1 - (\varepsilon_G)_{crit}}{(\varepsilon_G)_{crit}} U_G \tag{6}$$

where ε_G is the critical void fraction at which this transition occurs. It was assumed by Ullmann and Brauner that the void fraction marking the transition from Bubble flow, with spherical bubbles, to Slug flow, with elongated bubbles, can be obtained from simple geometrical considerations relating to the void fraction of trains of contacting bubbles. This led them to conclude that the Bubble-to-Slug transition would occur when the bubble diameter was *half* the pipe diameter, corresponding to a void fraction value of 0.16. However, a void fraction value of 0.15 was eventually used in the Ullmann and Brauner model.

3.3. Transition from Stratified-to-Annular flow

Ullmann–Brauner attributed the transition from Stratified-to-Annular flow to two mechanisms:

3.3.1. Loss of Stability of the Stratified flow structure

For thin liquid films flowing in horizontal pipes, the breakdown in Stratified flow occurs at a critical superficial gas velocity of:

$$U_G \geqslant C_1 \left[\frac{D\Delta\rho g, cos\beta + D\sigma k^2}{\rho_G}\right]^{0.5} \tag{7}$$

where k is the typical long wave number:

$$k \approx 2\pi/D \tag{8}$$

and

$$C_1 \approx 0.63\left(\frac{h}{D}\right)^{-0.25} \tag{9}$$

and h is the height of the liquid layer in a Stratified flow. The application of this criterion requires knowledge of the liquid layer thickness for given gas and liquid flow rates (assuming steady and fully developed Stratified flow)

3.3.2. Drop entrainment

Alternatively, it may be argued that the annular film is formed due to impingement of liquid drops, entrained from the wavy interface of the Stratified liquid layer by the inertia of the fast moving core gas flow. The critical relative velocity between the phases – leading to entrainment – was expressed as:

$$\Delta u_G = u_G - u_L \geqslant 4.36\left[\frac{\sigma\Delta\rho\cos\beta}{\rho_G^2}\right]^{1/4} F(on) \tag{10}$$

where

$$F(on) = \{1 + 1.443(N_{vd}\cos\beta)^{0.4}\}^{0.5} \tag{11}$$

and

$$N_{vd} = \frac{\mu_L^4\Delta\rho g}{\rho_L^2\sigma^3} \tag{12}$$

Ullmann and Brauner (2007) described these as two competing mechanisms. For a given liquid velocity, u_L, the smaller of the two predicted values of u_G, was assumed to dominate.

3.4. Transition from Slug-to-Annular flow

The transition from Slug-to-Annular flow was attributed by Ullman–Brauner to the prevention of *Wave Bridging*, which would otherwise act to deliver liquid from the lower layer to the upper layer of liquid, thus creating a liquid plug. To assure that such bridging does not occur, they determined that the superficial gas velocity, U_G, needed to exceed:

$$U_G \geqslant \tilde{\varepsilon}\left[\tilde{\varepsilon}\frac{\mu_L}{\mu_G} + 2\right]U_L \tag{13}$$

where

$$\tilde{\varepsilon} = \frac{1 - \varepsilon_L^{crit}}{\varepsilon_L^{crit}} \tag{14}$$

Ullmann and Brauner found an average liquid holdup (ε_L^{crit}) of 0.4 to be sufficient to maintain the Annular flow.

4. Empirical characterization of two-phase flow regimes in miniature tubes

4.1. Experimental apparatus

The experimental apparatus used to determine several two-phase flow characteristics of refrigerants flowing in miniature channels was located in the Heat and Mass Transfer Laboratory (LTCM), at the Swiss Federal Institute of Technology (EPFL); Revellin (2005) and Revellin et al. (2006). A total of more than 2200 observations were made and documented.

A microvalve was installed between the hot reservoir and the test section, before the preheater, in order to regulate the mass flow and avoid oscillations when boiling starts in the test section. This microvalve is designed to increase the pressure drop in the loop, so that back flow can be suppressed and a wider range of stable operating conditions achieved.

The refrigerant saturation temperature is adjusted by the pressure in the cold reservoir and the liquid subcooling is adjusted by the power provided to the preheater. The test loop, shown in Fig. 2, consists of an 80 mm long stainless steel tube used as a micro-preheater, a 20 mm long plastic tube for electrical insulation, followed by the micro-evaporator test section, which is a 110 mm long heated stainless steel tube. The micro-evaporator is followed by a 100 mm long glass tube for flow pattern visualization and optical measurements.

The internal diameters of the two glass test sections were 0.509 mm and 0.790 mm, respectively. Two copper clamps were attached to the micro-preheater and to the micro-evaporator. The clamps were connected electrically to two Sorensen power supplies and delivered direct current to heat the tubes. The heat flux provided to the test section was in the range of 3–415 kW/m^2. For further details on the experimental apparatus and data collected, the reader is referred to Revellin (2005) and Revellin et al. (2006).

4.2. Optical measurement technique

A method to determine the two-phase flow characteristics and flow pattern was developed at EPFL and is described in Revellin et al. (2006). The method consists of two, low-power (<1 mW) laser beams directed through both the glass visualization tube and the local fluid at two different locations. Two lenses focused the laser beams at the middle of the microtube. Two photodiodes measured the intensity of the light. The photodiodes were illuminated through a vertical 1 mm wide opening in the middle of the cover plate to isolate the signal. The photodiodes were connected to a National Instruments SCXI acquisition system using a scan rate of 10 kHz to measure the resulting voltage signals from the two diodes. A positioning system was used to align the laser beams with the lenses and photodiodes. The laser beams interact locally with the structure of the flow, thus making it possible to obtain the velocity, length, and frequency of vapor bubbles from signal processing. Fig. 3 shows an example of a voltage signal form a sin-

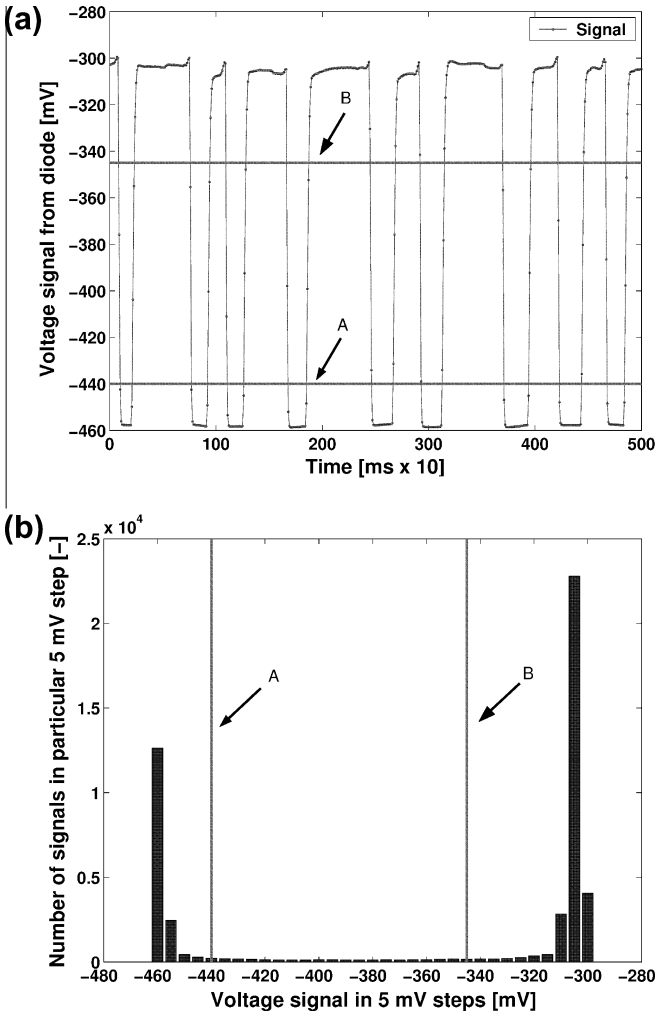

Fig. 3. (a) signal from a single diode versus time, and (b) histogram of 50,000 voltage signal segregated into 5 mV steps.

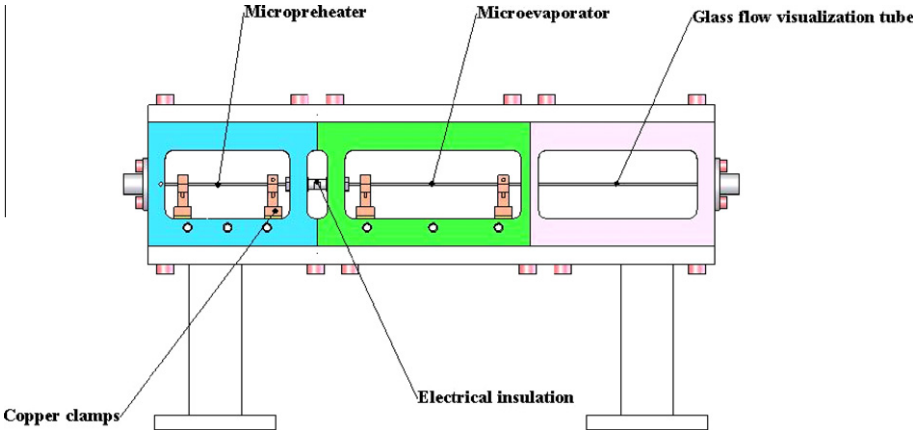

Fig. 2. Two-phase flow test section; preheater, evaporator, and the visualization section.

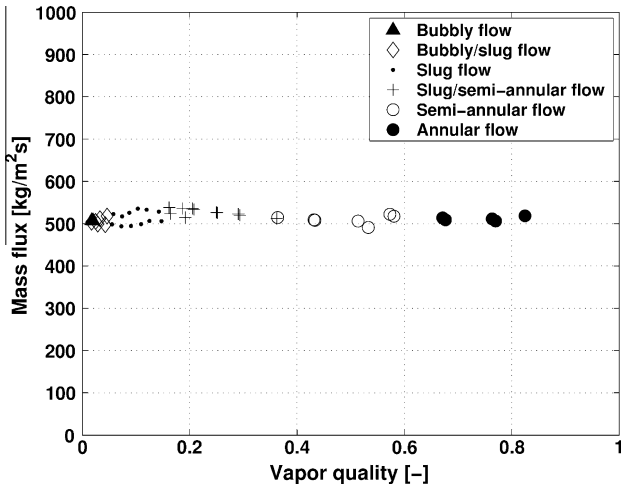

Fig. 4. Flow pattern determination from laser 1 for D = 0.509 mm, L_{MEV} = 70.70 mm, T_{sat} = 30 °C, G = 500 kg/m^{2}s, and T_{sub} = 3 °C. Data shown for increasing and decreasing heat flux.

gle diode and the histogram derived from the corresponding diode voltage signal.

Thresholds were determined in volts after first segregating the diode voltage signal into 5 mV steps. Limits were determined at 20 mV after the first peak for limit A and 40 mV before the second peak for limit B. Threshold A is −440 mV for this example and threshold B is −345 mV. When the voltage signal is below limit A, the presence of liquid is detected. Signals greater than limit B indicates that an Annular flow or an elongated bubble is present. Between these two thresholds, either the nose or tail of a bubble, or a frothy mix of liquid and vapor, is present.

As part of the experimental procedure, the heat flux was increased then decreased stepwise at a constant mass flux. It can be seen in Fig. 4 that increasing then decreasing the heat flux had no effect on the flow pattern detection. The uncertainties in the measured and derived values are listed in Table 1.

By examining the evolution of peak and valley bubble count rates versus vapor quality, it was possible to determine the rate

Table 1
Experimental conditions and uncertainties of the database.

Parameter	Range	Uncertainties	Units
Fluid	R134a, R245fa	–	–
D	0.509–0.790	±1.0%	mm
L	30–70	<2.5%	mm
G	210–2094	±2.0%	kg/m^{2}s
q	3.1–415	±5.5%	W/m^2
T_{sat}	26, 30, 35	±0.1	°C
P_{sat}	6.9, 7.7, 8.9 (R134a) 2.1 (R245fa)	<0.23%	bar
ΔT_{sub}	2–6	±0.2	K
x_{out}	0–0.95	±1.9%	–

of coalescence of small bubbles into elongated bubbles and elongated bubbles into Semi-Annular flow. The transitions were thus, in fact, detected by bubble count rates of signal peaks and valleys, relative to the A and B thresholds, and by the percentage of small bubbles remaining, as shown in Fig. 5.

Comparison of this method to video processing revealed that the relative error on the vapor velocity is less than 1%, as discussed by Revellin et al. (2006). In addition, the distance between the lasers was found to have a negligible influence on the results (Revellin, 2005) and the acquisition time has only a small influence on the bubble frequency and no effect on the cross-correlation (vapor velocity calculation). For all these reasons, the method is considered robust and accurate.

4.3. Flow patterns observed

Application of this optical bubble characterization technique yielded the following two-phase flow patterns:

4.3.1. Bubbly flow

The vapor phase in this flow regime is distributed as discrete bubbles in the continuous liquid phase and the bubbles are smaller in length than the diameter of the tube, Fig. 6a.

4.3.2. Bubbly/Slug flow

In this flow regime, the Bubbly flow (described above) and the Slug flow (described below) are both present, as shown in Fig. 6b.

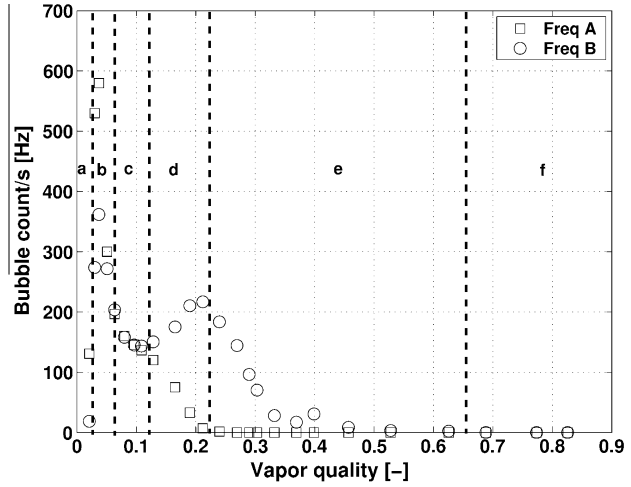

(A). Bubble frequencies and flow patterns, (a) Bubble flow, (b) Bubble/Slug flow, (c) Slug flow, (d) Slug/Semi-Annular flow, (e) Semi-Annular flow, and (f) Annular flow.

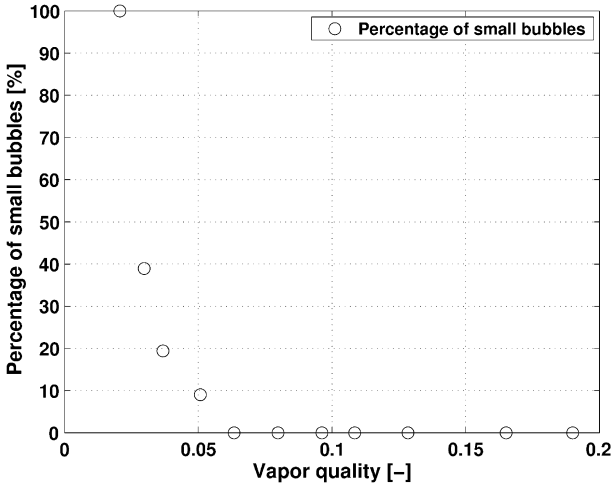

(B). Percentage of small bubbles remaining versus vapor quality.

Fig. 5. Characterization of flow using the laser signal for D = 0.509 mm, L_{MEV} = 70.70 mm, T_{sat} = 30 °C, G = 500 kg/m^{2}s, and T_{sub} = 3 K.

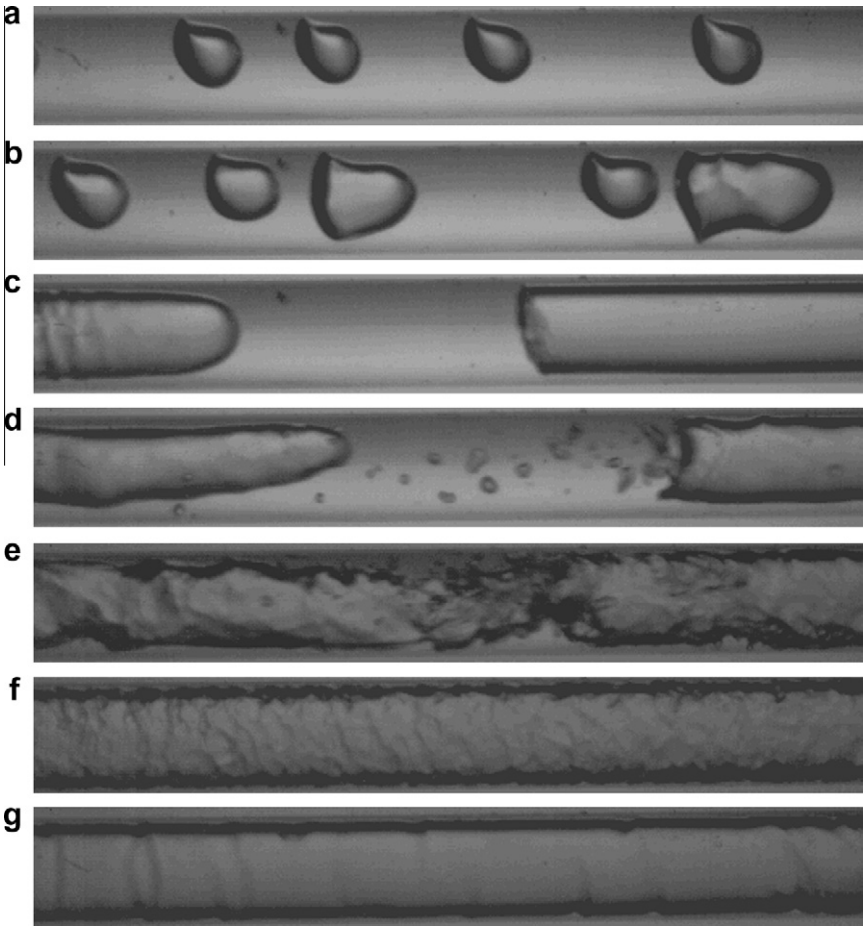

Fig. 6. Flow patterns and transitions for R134a, D = 0.790 mm, L_{MEV} = 70.70 mm, G = 500 kg/m^{2}s, T_{sat} = 30 °C, and T_{sub} = 3 K at the exit of the micro-evaporator. (a) Bubble flow at x = 0.03. (b) Bubble/Slug flow at x = 0.04. (c) Slug flow at x = 0.05. (d) Slug/Semi-Annular flow at x = 0.11. (e) Semi-Annular flow at x = 0.24. (f) Wavy Annular flow at x = 0.73. (g) Smooth Annular flow at x = 0.73.

4.3.3. Slug flow

The elongated vapor bubbles have approximately the same diameter as the tube and they grow in length as the flow proceeds downstream. The nose of the bubble has a characteristic hemispherical cap and the vapor in the bubbles is separated from the tube wall by a thin film of liquid. The liquid flow is contained mostly in the liquid "plugs," which separates successive vapor bubbles, as can be seen in Fig. 6c.

4.3.4. Slug/Semi-Annular flow

In this flow regime, the Slug flow (described above) and the Semi-Annular flow (described below) are both present. The vapor quality increases with heat flux and the rear of the elongated bubbles are more deformed – as shown in Fig. 6d. When coalescence occurs, the separation between the vapor slugs and liquid plugs are no longer clean but instead a churn-like zone is created between the slugs.

4.3.5. Semi-Annular flow

Semi-Annular flow is used to describe the flow pattern in which the churning liquid plugs, created by the previously discussed deformation of the "tails" of elongated bubbles and bubble coalescence, have almost disappeared and a nearly-continuous central vapor core has emerged. The churning liquid plugs gradually disappear from the beginning of this regime up to the end. The Semi-Annular flow pattern is shown in Fig. 6e.

4.3.6. Annular flow

In Annular flow, a liquid film flows on the tube wall with a continuous central vapor core as shown in Fig. 6f and g. It is the same definition as for Semi-Annular flow, except that the churning liquid zones no longer exist.

It is to be noted that no Stratified flow and nearly no bubble flow were detected in these experiments and that the majority of

Table 2
Flow regime terminologies.

Present study	Taitel–Dukler (1976)	Ullmann–Brauner (2007)	Revellin (2005)
Bubble	Bubble	Dispersed Bubbly, Bubbly	Bubbly, Bubbly/Slug
Slug	Slug–Intermittent	Slug, Aerated Slug	Slug, Slug/Semi-Annular
Annular	Annular	Annular	Semi-Annular, Annular

the observations fell in the Semi-Annular and Annular flow regimes.

For further information regarding the present data, the reader can refer to Revellin et al. (2006) and Revellin and Thome (2007a,b).

5. Comparison of empirical and theoretical flow regime maps

5.1. Flow regime definitions

To avoid the confusion that might arise from the variety of names used by different authors for the same flow regime, as well as the subtle differences associated with specific sub-regimes, a common flow regime terminology – defined in Table 2 – is used to compare the observed and predicted two-phase flow regimes. It is to be noted that when the Revellin (2005) sub-regimes are combined into the primary two-phase flow regimes, 182 of the 2239 data points fall in the Bubble regime, 895 in the Slug, and 1162 in the Annular flow regime.

Revellin (2005) observed that the transition from Slug flow to the Annular regime occurred when the rear of the elongated bubbles (i.e. slugs) began to deform and adjacent slugs began to coalesce, progressing to a continuous central vapor core and a liquid film at the tube wall. The Bubble-to-Slug transition was associated with the coalescence of the dispersed bubbles to form elongated bubbles which have approximately the same diameter as the tube.

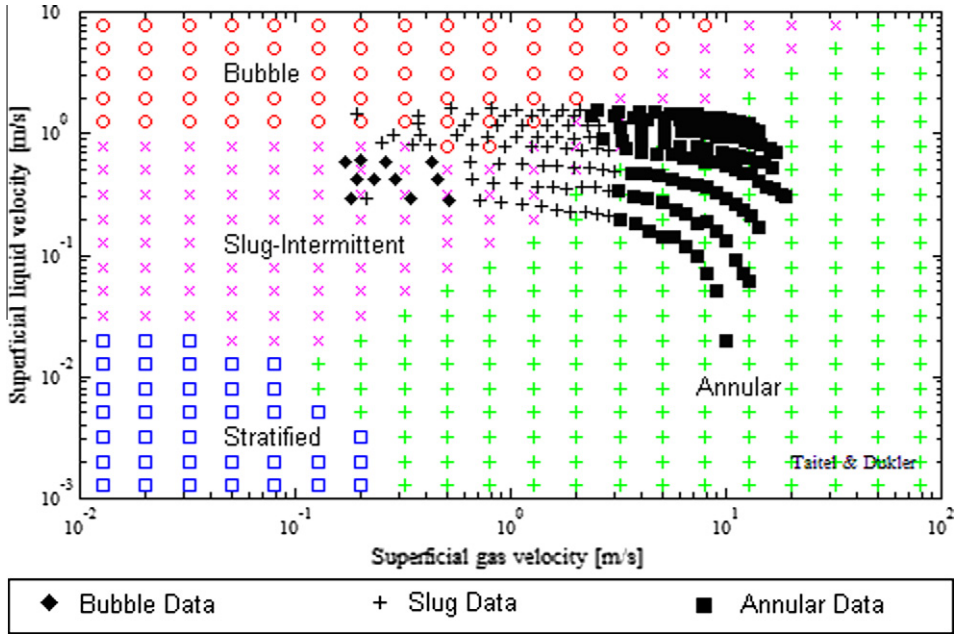

Fig. 7a. Taitel–Dukler flow regime map for data of R134a in 509 μm channel. T = 26 °C, $T_{\text{Inlet-sub}}$ = 3 K, G = 350–2000 kg/m^{2}s.

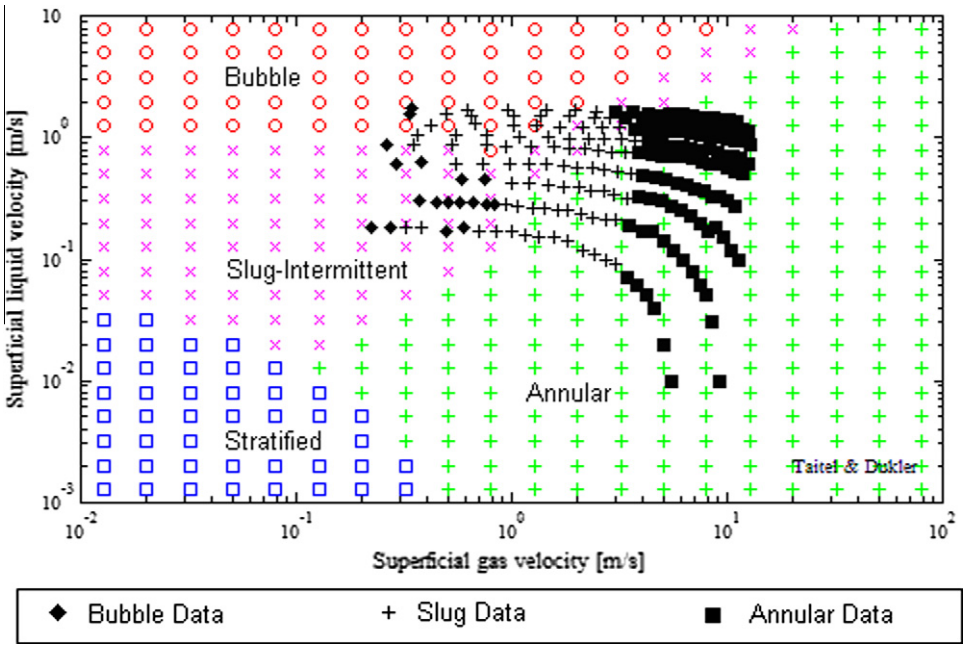

Fig. 7b. Taitel–Dukler flow regime map for data of R134a in 790 μm channel. T = 30 °C, $T_{\text{Inlet-sub}}$ = 3 K, G = 200–2000 kg/m^{2}s.

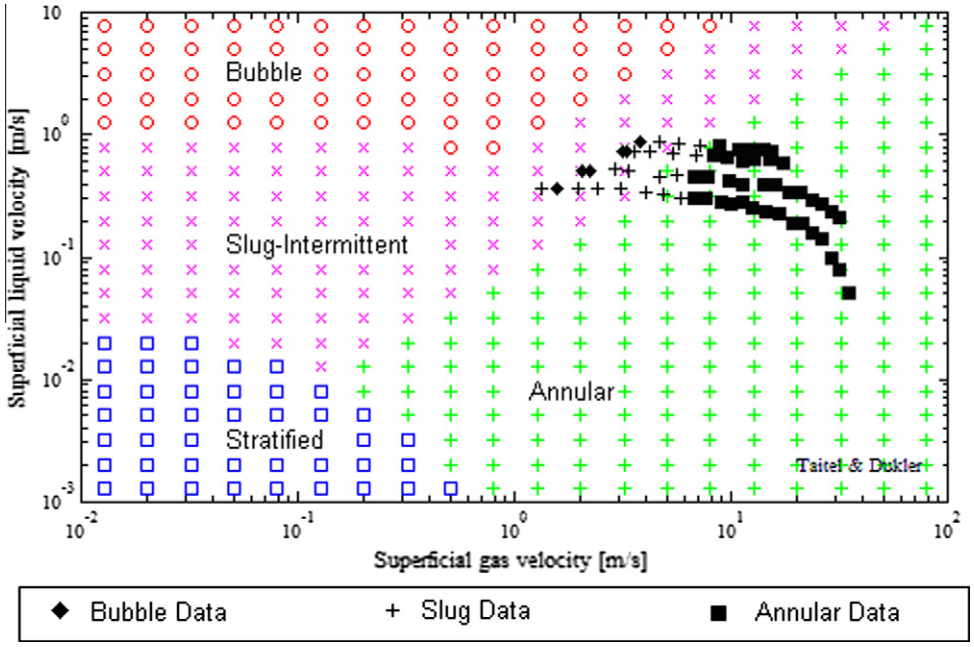

Fig. 7c. Taitel–Dukler flow regime map for data of R245fa in 509 μm channel. T = 35 °C, $T_{\text{Inlet-sub}}$ = 6 K, G = 500–1200 kg/m^{2}s.

5.2. Taitel–Dukler flow regime maps

The two-phase flow regime observations described above were compared to the predictions of the Taitel–Dukler flow regime map. As can be seen in Figs. 7a–7c displaying the loci of distinct mass fluxes with symbols chosen to reflect the experimentally observed flow regimes, in each of three operating conditions, agreement in the dominant flow regimes can be observed between the data and the Taitel–Dukler model. Expanding this comparison to include the full Revellin (2005) dataset of flow regime observations, revealed that 67% of the 2239 empirically observed flow pattern data were in the theoretically predicted regime. However, it must be noted, that the location and slope of the observed Bubble-to-Slug transition boundary, with a somewhat sparse data sub-set, is not well predicted by Taitel–Dukler. Thus, 48% of the Slug data and 92% of the Annular data, but only 2% of the limited Bubble data, is correctly predicted by Taitel–Dukler.

5.3. Ullmann–Brauner model

The empirical regime observations were next compared to the Ullmann–Brauner two-phase flow regime predictions, based on

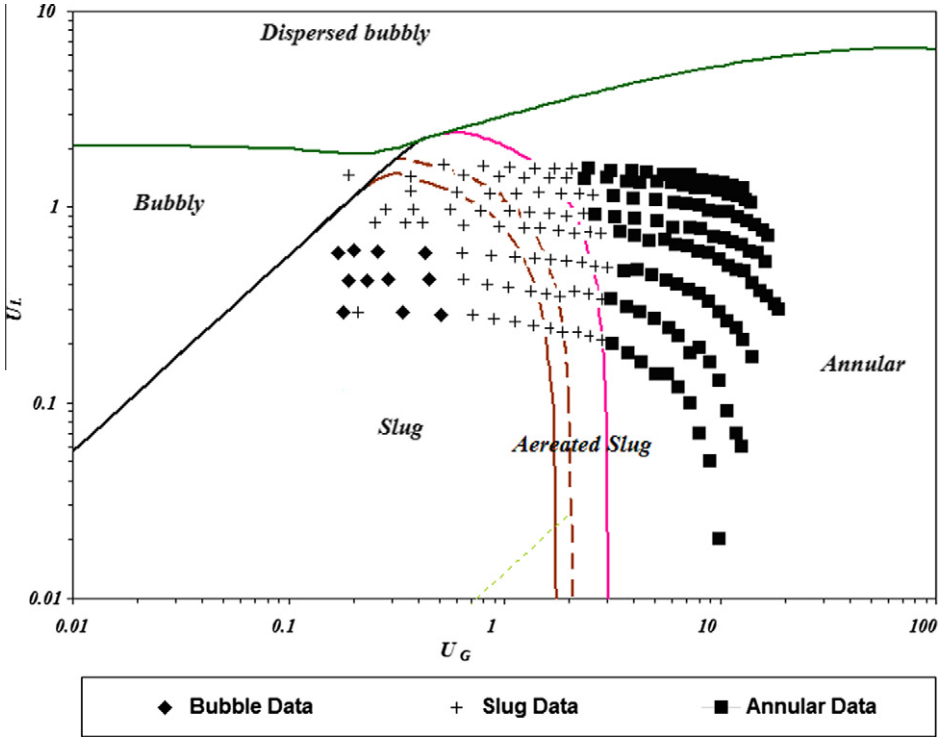

Fig. 8a. Ullmann–Brauner flow regime map for data of R134a in 509 μm channel. T = 26 °C, $T_{\text{Inlet-sub}}$ = 3 K, G = 350–2000 kg/m^{2}s.

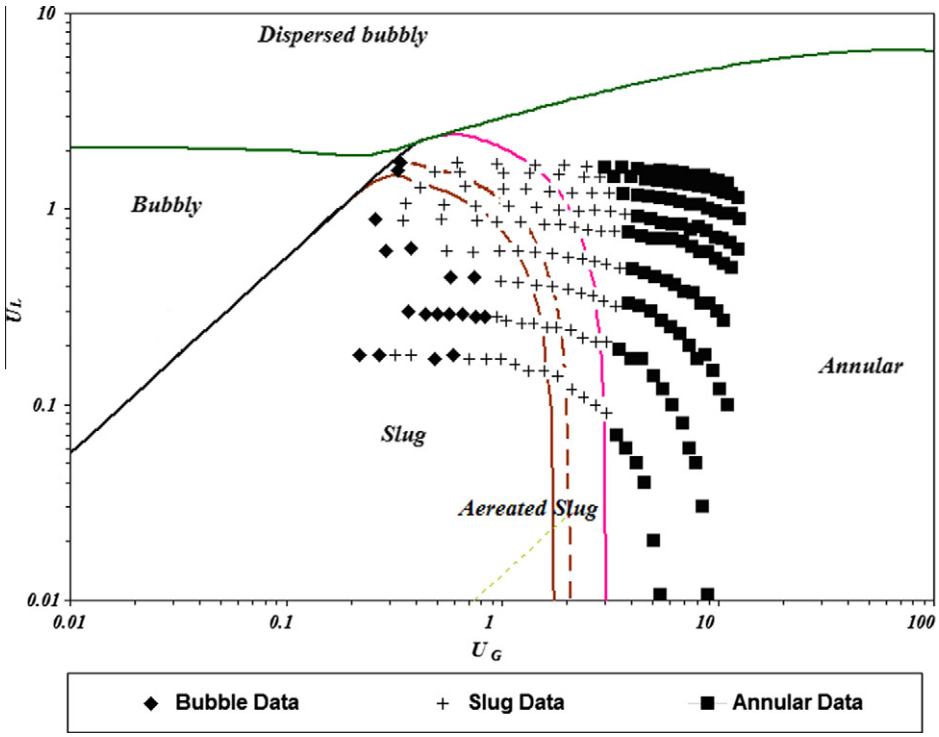

Fig. 8b. Ullmann–Brauner flow regime map for data of R134a in 790 μm channel. T = 30 °C, $T_{\text{Inlet-sub}}$ = 3 K, G = 200–2000 kg/m^{2}s.

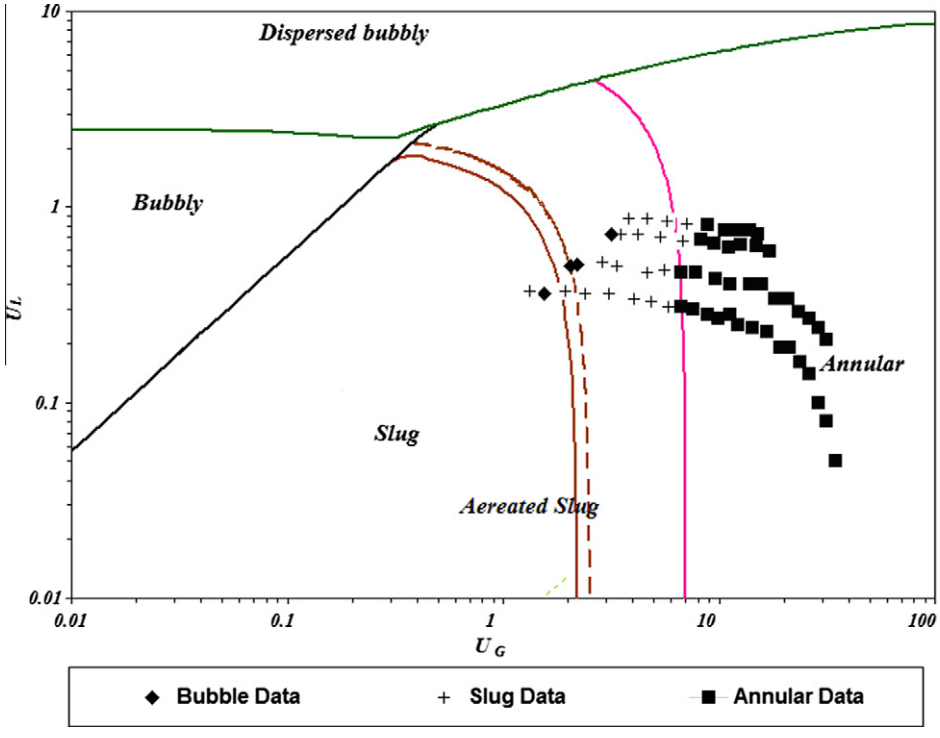

Fig. 8c. Ullmann–Brauner flow regime map for data of R245fa in 509 μm channel. T = 35 °C, $T_{\text{Inlet-sub}}$ = 6 K, G = 500–1200 kg/m^{2}s.

their proposed Bubble-to-Slug, Stratified-to-Annular, and Slug-to-Annular flow regime transitions. As may be seen in Figs. 8a–8c, the Slug-to-Annular transition is nearly vertical at low superficial liquid velocities and curves to the left at higher values of the liquid superficial velocity, as the Bubble flow regime is approached. Interestingly, this curvature in the Slug-Annular boundary does not appear to improve the predictability of the flow regimes prevailing in the Revellin et al. test sections. It is also to be noted that, while the

transition boundary from Bubble flow to Slug flow appears to display the appropriate slope, it is far to the left of the empirically observed transition.

Despite these discrepancies, the Ullmann–Brauner model correctly predicted the appropriate flow regime for 81% of the full Revellin (2005) dataset of flow regime observations. The Ullmann–Brauner model achieved this accuracy by offering improved predictability in the Annular and Slug regimes, relative to Taitel and Dukler, properly accounting for 99% of the Annular data and 74% of the Slug data, respectively, but failing to correctly identify any of the 182 Bubble data points. While the Ullmann–Brauner model was, thus, better able to predict the location and slope of the Slug-to-Annular transition than Taitel–Dukler, for the smaller diameter tube (0.509 mm), it predicted the transition to Annular flow to occur at a lower vapor quality than observed in this study.

5.4. Flow regime map modifications for miniature channels

The preceding has established the efficacy of using the classical Taitel–Dukler map to determine the prevailing flow regimes in the two-phase flow of refrigerants in miniature tubes. Despite the significant difference in scale between the majority of the data originally used to validate the Taitel–Dukler regime transitions and the sub-millimeter tubes studied herein, the dominant regime (Annular flow) and nearly 67% of the observations, were correctly identified by the Taitel–Dukler methodology. Modifications to the Bubble-to-Slug, Stratified-to-Annular, and Slug-to-Annular flow regime transitions, proposed by Ullman and Brauner (2007) yielded a further improvement and correctly identified the flow regime of 81% of the miniature tube observations.

5.4.1. Modified bubble-to-intermittent transition

As previously noted, while the Ullmann–Brauner transition from Bubble flow to Slug flow appears to display the appropriate slope, it is far to the left of the empirically observed transition for the miniature tubes studied herein. However, when Eq. (6) is modified to allow transition when the critical void fraction is 0.67, i.e. the diameter of the bubble is essentially equal to the tube diameter, the boundary moves to the right, as in Figs. 9a–9c, capturing much of the observed Bubble data at mass fluxes of ($G \leqslant 700$ kg/m^{2}s), i.e. 123 out of the 182 Bubble data points at low mass flux are now correctly predicted, yielding an agreement of 68%. However, the use of the revised Bubble-to-Slug transition boundary over the entire range of mass fluxes yielded less satisfactory results, since many of the Slug data points were falling in the Bubble region at moderate and high mass fluxes ($G > 700$ kg/m^{2}s).

5.4.2. Modified intermittent to Annular transition

As is visible in Figs. 9a and 9c, the nearly vertical *U-B* Slug-to-Annular transition at low mass fluxes is consistent with the shape of the empirically-observed boundary between these two regimes and some discrepancies are generated by the "curvature" of this boundary to the left and lower gas superficial velocities at the higher mass fluxes. Interestingly, setting the transition from Slug-to-Annular to occur as a vertical line at a superficial vapor velocity equivalent to that where the transition occurs at low mass flux ($G \leqslant 500$ kg/m^{2}s) results in a significant improvement in the predictive accuracy, with a greater fraction of the Slug data properly categorized, and the prediction accuracy raising from 74% to 84%.

Implementing this change yields an average accuracy of 84% for the Slug data and 99% for the Annular data, which results in an overall accuracy improvement from 88% to 92% for the combined Slug and Annular data.

An example of the proposed modifications in the flow regime map is shown in Figs. 9a and 9c.

5.5. Specific parametric dependencies

To complete the comparison of observed and predicted flow regime transitions, the specific parametric dependencies associated with mass flux, fluid properties, saturation temperature, inlet subcooling, and tube diameter were examined, with the use of the modified flow regime map.

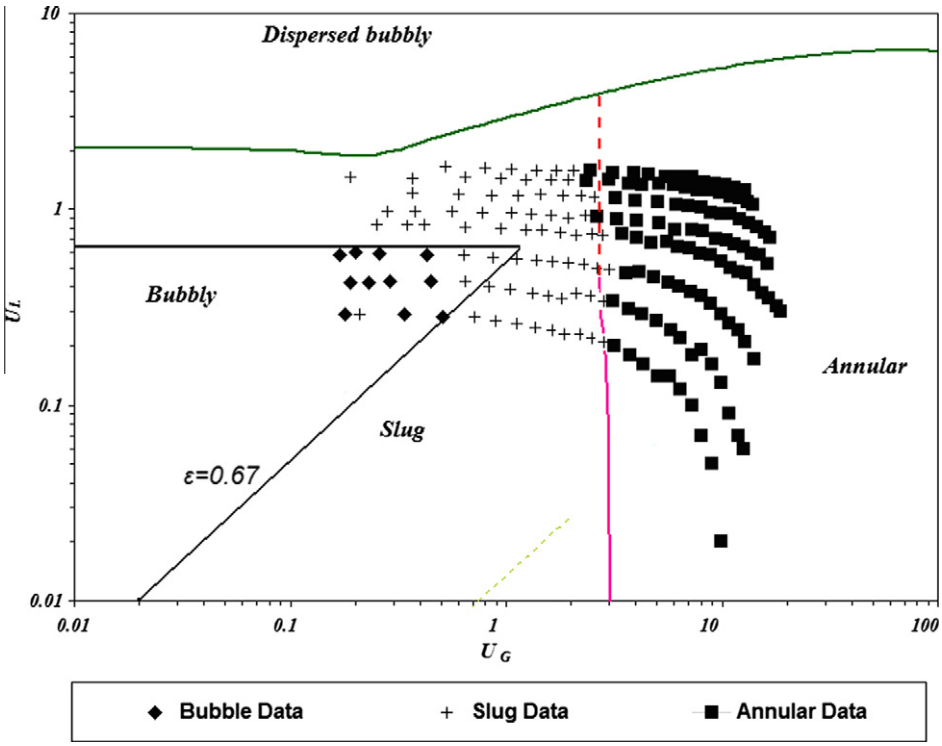

Fig. 9a. Ullmann–Brauner flow regime map, with modified transition boundaries, for data of R134a in 509 μm channel. $T = 26$ °C, $T_{\text{Inlet-sub}} = 3$ K, $G = 350$–2000 kg/m^{2}s.

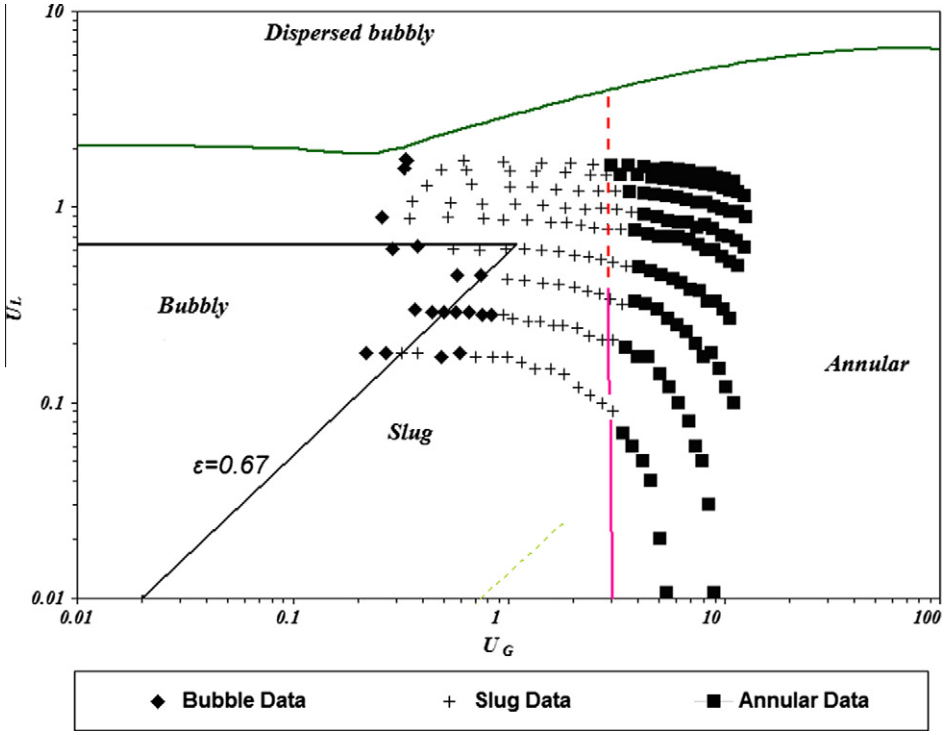

Fig. 9b. Ullmann–Brauner flow regime map, with modified transition boundaries, for data of R134a in 790 μm channel. T = 30 °C, $T_{\text{Inlet-sub}}$ = 3 K, G = 200–2000 kg/m^{2}s.

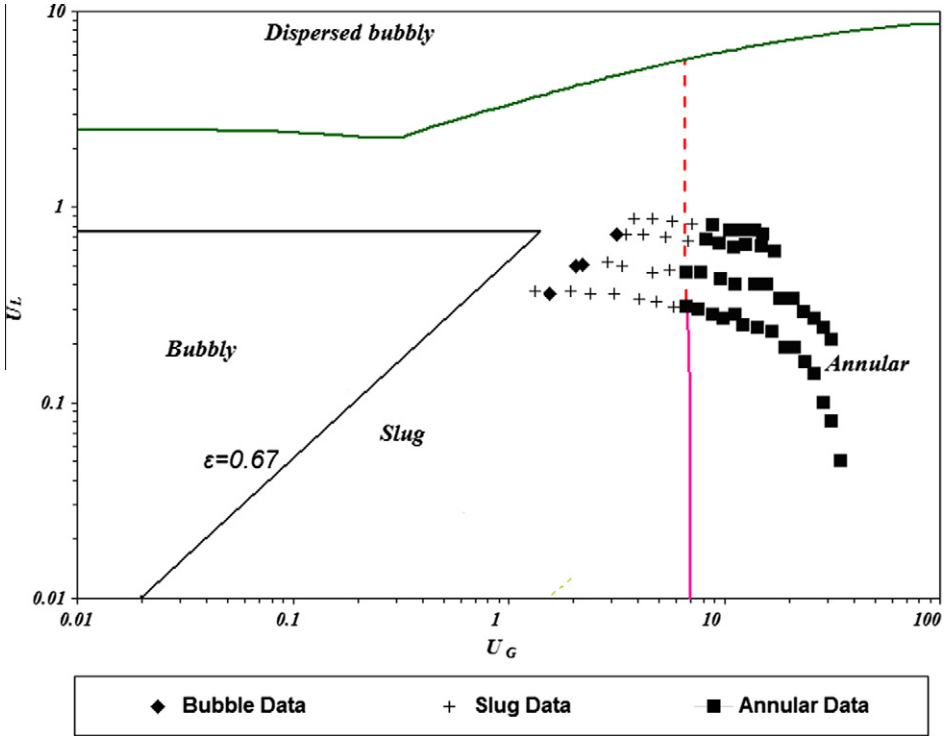

Fig. 9c. Ullmann–Brauner flow regime map, with modified transition boundaries, for data of R245fa in 509 μm channel. T = 35 °C, $T_{\text{Inlet-sub}}$ = 6 K, G = 500–1200 kg/m^{2}s.

5.5.1. Mass flux

The data were divided into three ranges of mass flux: low mass flux (200–500 kg/m^{2}s), moderate mass flux (700–1500 kg/m^{2}s) and high mass flux (1800–2000 kg/m^{2}s). It was found the best Taitel–Dukler predictions occurred for the low and moderate mass flux data, with the ability to predict the correct regime for 61% and 75% of these data points. This predictability was as low as 54% for the data points in the high mass flux range.

The best range of predictions by the Ullmann–Brauner model was achieved for the moderate mass flux data. The percentages of data points predicted correctly were 75%, 84%, and 83% for the low, moderate, and high mass flux data, respectively.

5.5.2. Fluid properties

The two fluids used in the present study, R134a, and R245fa, have a considerable difference in surface tension, a key parameter in two-phase physics (see for instance, Tabatabai and Faghri, 2001), with the surface tensions of R134a and R245fa equaling 0.007 N/m and 0.013 N/m, respectively.

It was found that the Taitel–Dukler map performed with better accuracy for R245fa than R134a, while the predictions of the Ullmann–Brauner model was nearly unaffected by this variable. Taitel–Dukler predicted the correct flow regime for 185 of the 235 R245fa data points or 79%, and 1320 out of the 2004 R134a data points for an accuracy of 66%. Ullmann–Brauner predicted correctly 83% of the R245fa data points and 81% of the R134a data points.

5.5.3. Saturation temperature and Inlet subcooling

The experiments examined in this study were run at three different values of saturation temperatures (25, 30, and 35 °C) with the inlet subcooling ranging from 2 to 6 K. It was observed that the saturation temperature has a noticeable effect on the models' predictions: Taitel–Dukler providing the correct regimes for 67%, 64%, and 72% of the data points at saturation temperatures of 25, 30, and 35 °C, respectively. Ullmann–Brauner model performed best when predicting the flow regime for the 25 °C inlet temperature data, with 91% accuracy, while the 30 °C and 35 °C data is predicted with 77% and 85% accuracy, respectively.

As expected, the influence of the relatively small subcooling on the flow regimes exiting the micro-evaporator channel was very limited for both models, with no significant variation in the prediction discrepancy for the different values of inlet subcooling.

5.5.4. Tube diameter

The current database consists of 1591 data points in a 0.509 mm diameter tube, and 648 data points in a 0.790 mm diameter tube. It was found for the present dataset that both existing models predicted the correct regime with better accuracy for the smaller tube. The Taitel–Dukler model predicts the correct regime with an accuracy of 70% and 62%, for the 0.509 mm and 0.79 mm data, while the Ullmann–Brauner model prediction accuracy is 86% and 70%.

6. Conclusions

Observed two-phase flow patterns for R134a and R245fa in tubes with inner diameter of 0.509 mm and 0.790 mm were compared to the predictive analytical models of Taitel and Dukler (1976), Taitel et al. (1980), and Ullmann and Brauner (2007). Among the 2239 flow regime data points, no Stratified flow was observed and a small number of bubble flow data existed, with Annular flow and the Slug (Intermittent) flow dominating. The Taitel–Dukler model predicted the correct regime for 67% of the data points, while the Ullmann–Brauner model predicted the correct regime for 81% of the total data points.

Despite the highly-satisfactory overall predictive accuracy of the Ullmann–Brauner regime boundaries, it was found that this model predicted the Bubble-to-Slug flow transition with a very large discrepancy and displayed progressively poorer agreement with the Slug-to-Annular transition as the mass flux increased.

Despite a modified transition boundary not affecting the prediction accuracy for Annular data (remained at 99%), a vertical transition boundary improved the prediction accuracy for Slug data from 74% to 84%.

Similarly, modifying the *U-B* Bubble-to-Slug transition to occur when the bubble diameter equals the full tube diameter, can bring the overall agreement from 0% to 68%.

Overall, applying the modified Bubble-to-Slug and Slug-to-Annular transition boundaries yields an improved overall agreement of 90%.

References

Baker, O., 1954. Simultaneous flow of oil and gas. Oil Gas J. 53 (12), 185–195.

Bar-Cohen, A., Rahim, E., 2009. Modeling and prediction of two-phase microgap channel heat transfer characteristics. Heat Transfer Eng. 30 (8), 601–625.

Bar-Cohen, A., Ruder, Z., Griffith, P., 1987. Thermal and hydrodynamic phenomena in a horizontal uniformly heated steam generating pipe. J. Heat Transfer 109, 739–745.

Barnea, D., Shoham, O., Taitel, Y., Dukler, A.E., 1980. Flow pattern transition for gas–liquid flow in horizontal and inclined Pipes. Int. J. Multiphase Flow 6, 217–226.

Cheng, L., Ribatski, G., Thome, J.R., 2008. Two-phase flow patterns and flow-pattern maps: fundamentals and applications. Appl. Mech. Rev., 61, Paper # 050802.

Frankum, D.P., Wadekar, V.V., Azzopardi, B.J., 1997. Two-phase flow patterns for evaporating flow. Exp. Thermal Fluid Sci. 15, 183–192.

Harirchian, T., Garimella, S., 2008. An investigation of flow boiling regimes in microchannels of different sizes by means of high-speed visualization. In: Proceedings of ITherm, 2008.

Hewitt, G.F., 1982. Liquid–gas systems, flow regimes. In: G. Hetsroni (Ed.), Handbook of Multiphase Systems, Sec. 2-3–2-43. Hemisphere, Washington, D.C.

Kattan, N., Thome, J.R., Favrat, D., 1998. Flow boiling in horizontal tubes. Part 3: development of a new heat transfer model based on flow patterns. J. Heat Transfer 120 (1), 156–165.

Mandhane, J.M., Gregory, G.A., Aziz, K., 1974. A flow pattern map for gas liquid flow in horizontal pipes. Int. J. Multiphase Flow 1, 534–553.

Megahed, A., Hassan, I., 2009. Two-phase pressure drop and flow visualization of FC-72 in a silicon microchannel heat sink. Int. J. Heat Fluid Flow 30, 1171–1182.

Revellin, R., 2005. Experimental Two-phase Fluid Flow in Microchannels. PhD. Thesis (Prof. John R. Thome, Director), LTCM-EPFL, Swiss Federal Institute of Technology. <http://library.epfl.ch/theses/?nr=3437>.

Revellin, R., Thome, J.R., 2007a. Experimental investigation of R-134a and R-245fa two-phase flow in microchannels for different flow conditions. Int. J. Heat Fluid Flow 28, 63–71.

Revellin, R., Thome, J.R., 2007b. New type of diabatic flow pattern map for boiling heat transfer in microchannels. J. Micromech. Microeng. 17, 788–796.

Revellin, R., Dupont, V., Ursenbacher, T., Thome, J.R., Zun, I., 2006. Characterization of two-phase flows in microchannels: optical measurement technique and flow parameter results for R-134a in a 0.5 mm channel. Int. J. Multiphase Flow 32, 755–774.

Revellin, R., Agostini, B., Thome, J.R., 2008. Elongated bubbles in microchannels, part II: experimental study and modeling of bubble collisions. Int. J. Multiphase Flow 34, 602–613.

Shoham, O., 1982. Flow Pattern Transition and Characterization in Gas–liquid Flow in Inclined Pipes. PhD. Dissertation, Tel-Aviv University, Ramat-Aviv, Israel.

Tabatabai, A., Faghri, A., 2001. A new two-phase flow map and transition boundary accounting for surface tension effects in horizontal miniature and micro tubes. J. Heat Transfer 123 (5), 958–968.

Taitel, Y., 1990. Flow pattern transition in two phase flow. In: Proceedings of the 9th International Heat Transfer Conference, pp. 237–254.

Taitel, Y., Dukler, A.E., 1976. A model for predicting flow regime transitions in horizontal and near horizontal gas–liquid flow. AIChE J. 22 (1), 47–55.

Taitel, Y., Dukler, A.E., 1987. Effect of pipe length on the transition boundaries for high viscosity liquids. Int. J. Multiphase Flow 13, 577–581.

Taitel, Y., Barnea, D., Dukler, A.E., 1980. Modelling flow pattern transitions for steady upward gas–liquid flow in vertical tubes. AIChE J. 26 (3), 345–354.

Taitel, Y., Lee, N., Dukler, A.E., 1978. Transient gas–liquid in horizontal pipes: Modeling the flow pattern transitions. AIChE J. 24, 920–934.

Triplett, K.A., Ghiaasiaan, S.M., Abdel-Khalik, S.I., Sadowski, D.L., 1999. Gas-liquid two-phase flow in micro-channels, part 1: two-phase flow pattern. Int. J. Multiphase Flow 25, 377–394.

Ullmann, A., Brauner, N., 2007. The prediction of flow pattern maps in mini channels. Multiphase Sci. Technol. 19 (1), 49–73.

Weisman, J., Duncan, D., Gibson, J., Crawford, T., 1979. Effect of fluid properties and pipe diameter on two-phase flow pattern in horizontal lines. Int. J. Multiphase Flow 5, 437–462.

Yang, Y., Fujita, Y., 2004. Flow boiling heat transfer and flow pattern in rectangular channel of mini-gap. In: Proceedings of the 2nd International Conference on Microchannels and Minichannels, New York, USA, Paper no. ICMM2004-2383.